International Journal of Heat and Mass Transfer 216 (2023) 124557

Contents lists available at ScienceDirect

International Journal of Heat and Mass Transfer

journal homepage: www.elsevier.com/locate/ijhmt

Spectral Heat Transfer Coefficient for convection

L. He

Department of Engineering Science, University of Oxford, United Kingdom

ARTICLE INFO

Keywords:
Convective heat transfer
Heat transfer coefficient
Fourier method
Conjugate heat transfer
Non-isothermal wall

ABSTRACT

The present work is aimed at developing a methodology to predict convective heat transfer of flow bounded by a non-isothermal wall, which has been a long-standing issue of interest for Newton's law of cooling. A framework is proposed to centre around the Spectral Heat Transfer Coefficients (SHTC). They are effectively global-to-local temperature-heat flux influence coefficients for a small number of low order spectral modes of wall temperature disturbances for a range of physically relevant and numerically resolvable length scales. The framework is implemented with a unified Fourier spectral method applicable to both spatially periodic and non-periodic wall temperature distributions. The Fourier spectral formulation also leads to the zeroth harmonic base mode corresponding to exactly the standard form of Newton's law of cooling, thus the method is directly applicable to both non-isothermal and isothermal cases, as intended. The method formulations in both 2D and 3D settings and the working procedure are presented. All computational case studies for 2D and 3D configurations clearly and consistently demonstrate the validity and effectiveness of the proposed framework methodology and method implementation.

1. Introduction

1.1. General background and problem statement

Convective heat transfer is of great relevance to a wide range of problems. The most widely used treatment/wisdom has been based on Newton's law of cooling. The original form of $q \propto (T\text{-}T_a)$ for heat flux q, solid metal temperature T, and ambient air temperature T_a, underlines the most fundamental and useful assumption of linearity. The standard form for a flow of free stream temperature T_f, bounded by a solid wall of surface temperature T_w is:

$$q = h\left(T_w - T_f\right) \tag{1.1}$$

where the coefficient of proportionality is the heat transfer coefficient (HTC). It follows that HTC should be completely determined by flow, independent of the wall temperature. Effectively, in this context HTC is regarded as a wall-temperature 'invariant descriptor' for convective heat transfer, the term sometimes used to underscore that HTC and the like are only dependant on the fluid mechanics [1]. This has been the basic principal wisdom in conventional treatment of convective heat transfer.

Although linearity in terms of HTC independence of T_w may be questioned in some cases where the influence of wall temperature conditions on fluid flow becomes non-negligible (e.g. [2–5]), it is recognised that for many applications of practical interest, linearity is more than adequately justifiable, and thus is taken as the basic assumption and a justifiable starting point here for the present work.

A long-standing issue of more general interest and wider practical relevance is related to the temperature distribution over the solid wall boundary. It is understood that Newton's law of cooling in its original form had been established experimentally for an isothermal wall (T_w = constant over the entire wall boundary surface). Although it may be tempting to apply it to more general cases, there is no established basis for Newton's law of cooling in its original form to be applicable for non-isothermal walls. The simplicity and the power of the linear proportionality (thus superpositionality) of Newton's 'law' as we know it clearly appeal. However, the applicability of Newton's law of cooling (in its original or extended form) for general non-isothermal cases remains one of the major issues in the field of convective heat transfer. There has been a long-term quest in search for wall-temperature 'invariant descriptors' and working methods for convective heat transfer over non-isothermal walls, e.g. as overviewed by Moffatt [1].

Noticeable however is that the question mark regarding the applicability of Newton's law of cooling does not seem to stop attempts trying to apply it to non-isothermal walls. A common mode of applications in convective heat transfer is to scale HTC obtained in one condition (e.g. a low temperature lab testing or an empirical correlation) to a different

E-mail address: li.he@eng.ox.ac.uk.

https://doi.org/10.1016/j.ijheatmasstransfer.2023.124557
Received 28 April 2023; Received in revised form 8 July 2023; Accepted 29 July 2023
Available online 27 August 2023

condition (e.g. a high temperature operational condition) through non-dimensional parameters (e.g. Nusselt number, Biot number). It is not uncommon to see that an HTC obtained in an isothermal condition is either directly used in another non-isothermal condition or scaled through the non-dimensional parameters to other non-isothermal conditions. Sometimes, we may experience rather large uncertainties in the HTC scalability or inconsistent Nusselt numbers for seemingly similar geometric and flow conditions. In some cases, various measures may be identifiable to mitigate the large uncertainties and inconsistency, e.g. by finding less sensitive reference or averaged parameters when scaling through a non-dimensional one (e.g. [6,7]). A more relevant and searching question might be: is HTC in Newton's law of cooling 'fit for purpose' fundamentally for the problem in point?

Here we consider a simple example to see how uncertain an isothermal HTC can be if used for a non-isothermal case. Take a simple canonical setting of a 2D laminar boundary layer on a flat plate (Re=1000 based on the free stream velocity and the plate length). The present author computed the heat flux with an in-house CFD code. Firstly, two isothermal wall cases are considered, with the second case subject to a doubled magnitude of the constant wall temperature disturbance (T_w-T_f) of the first one. Fig. 1a shows the streamwise friction coefficient distribution, compared against the Blasius analytical solution as the basic validation for the calculations. The practically identical results of the two cases subject to the two different thermal conditions confirm the flow independence of the wall heat transfer, as assumed. The local Nusselt number distributions for the two wall temperature conditions also show a good linear behaviour and are in good agreement with the analytical solution (Fig. 1b).

However, following the same procedure for the same flow field but subject to a streamwise sinusoidal wall temperature profile, we see a very different picture (Fig. 2). The agreement in the Nusselt number

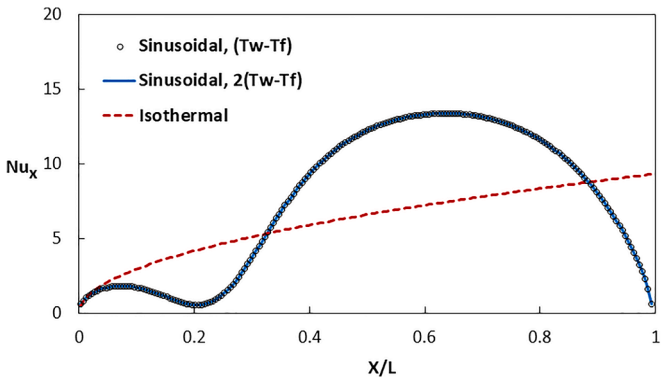

Fig. 2. Flat plate boundary layer subject to heat transfer with a non-isothermal wall.

(non-dimensional heat fluxes) between the two different magnitudes of the wall temperature disturbances confirm that the cases are still in a perfectly linear regime. Note that linearity is a necessary but not sufficient condition for the validity of the law of cooling. The results for the two non-isothermal cases seemingly show that they are scalable in terms of the magnitude. But this observed scalability is only valid for the cases with exactly the same non-isothermal wall temperature profile, so it would be of little use generally. In fact, the disagreement of the non-isothermal case with the isothermal one, as illustrated in Fig. 2, cannot be clearer. The differences in Nusselt number (normalised HTC) give a direct indication of the level of differences in the heat transfer prediction, should the same HTC obtained in the first isothermal case be used in the second non-isothermal one.

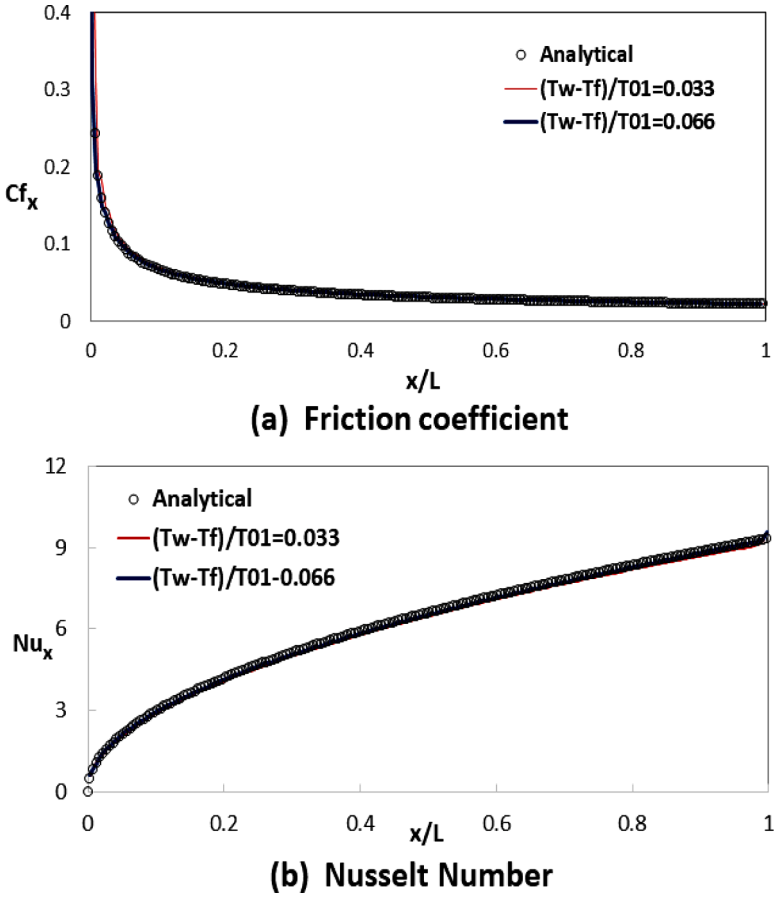

Fig. 1. Flat plate boundary layer subject to heat transfer with an isothermal wall.

There should be no doubt that the HTC obtained in an isothermal setting is not applicable for non-isothermal conditions with errors deemed to be too large to be acceptable in general. The need for alternative frameworks and working methods for convective heat transfer over non-isothermal wall is firmly underlined.

1.2. Some related work and main outstanding issues

Ever since Newton's paper was published 300 years ago, there have been numerous publications examining the validity of Newton's law of cooling. Some notable publications have appeared even in the past 60 years or so (e.g. [8–11], and others as reviewed by Besson [12]). Most of them however are mainly focused on its validity and accuracy for an experimental isothermal setup with a spatially uniform temperature, as much as practically possible, such as a latest example by Maruyama and Moriya [13] as recent as in 2021). Suffice to say that there has not been any systematically established evidence to challenge the validity of the 'law' as it is for an isothermal wall setting.

Many practical applications are not isothermal even approximately, and the HTC obtained from isothermal conditions (as often the case) are not applicable, as illustrated for even a very simple example above. The challenge for non-isothermal walls has been long recognised, though perhaps not as widely discussed in open literature as one might expect given its fundamental and general nature. A notable example is the paper by Moffat [1], having clearly and emphatically stated the inadequacy of the isothermal HTC for non-thermal cases, and stressed the need of the quest for a general true wall-temperature 'invariant descriptor' (as the standard HTC might be regarded or assumed conventionally) for convective heat transfer.

The central point recognised is that the wall heat flux at a given location can be influenced by other parts of the wall. Thus, the original simple form of the Newton's law of cooling may not be applicable to non-isothermal cases. One of the potential candidate methods identified then in [1] is 'Discrete Green's Function', first proposed by Hacker & Eaton [14]. A principally similar but different approach was also pursued earlier by Anderson and Moffat [15]. The discrete Green's function approach was subsequently followed chiefly experimentally in [14–20]. The method has been more recently further developed by Eaton [21] and Hoffman and Eaton [22].

The Green's function-based formulations do provide complete wall-temperature 'invariant descriptors', thus are of great potential to be advantageous in general over the standard form of Newton's law of cooling. However, Green's functions (even in a discrete form) are quite challenging to generate computationally (and experimentally). Note that Green's functions in a discrete form are effectively local influence coefficients at a mesh-size level, as shown by He [23], which may in principle be obtainable by computing (or measuring) thermal responses to each local temperature impulse disturbance of a mesh-size scale for all wall boundary mesh points. Analytical formulations of discrete Green's functions may be generated for simplified configurations and conditions (e.g. [21]).

However, general CFD methods are not quite amendable to directly solving the Green's functions. A fine mesh is commonly used to resolve relevant disturbances of small length scales which nevertheless will still have to be longer than the mesh-spacing. There is a conundrum for CFD both in accuracy and computational cost when directly solving the Green's functions. Firstly, regardless of the mesh density adopted, CFD methods inherently lack the differentiating capability to resolve the local temperature impulse disturbance in a length-scale of its own mesh spacing. Secondly, of all influences from all mesh elements over a wall surface, the strongest influence (the largest magnitude of Green's function) on a mesh point may be from the very mesh-element itself. Hence, if we take a much coarser partition in setting up the thermal impulse disturbances, there will be considerable uncertainties due to the low resolution both in the set thermal disturbances and in the computed local responses for the mesh point concerned.

In terms of computational resources required, it will be very costly for CFD-type solutions as every mesh point on a wall surface may be influenced by all other mesh points on the surface. Consider a 3D domain bounded by a discretised solid surface of M and N mesh points in the two wall-parallel directions. Direct MxN field calculations are then required for generating Green's functions for MxN surface mesh points. Correspondingly there will be a memory increase of $(MxN)^2$.

1.3. Present aims and work scope

The present work is motivated by the recognition of the need for new working methods in the context of Newton' law of cooling for non-isothermal walls, and the state of art and issues of relevance in the Green's function-based method development. More specifically, if we can manage to reduce the problem size of finding Green's functions by one order of magnitude in each wall-parallel direction respectively, we shall be able to get equivalently two orders of magnitude reduction in the total number of calculations needed and four orders of magnitude memory saving.

In fostering a method development, we intend to have two major desired attributes. First, it is underlined that the main difficulty in obtaining the Green's functions directly arises from the locality of the functions. Hence, in contrast to the local-to-local short-scale influences as in the basic Green's function formulation, a primary intent of the present work is to start from a global large-scale, and refine the scales systematically and efficiently to local small but also mesh-resolvable scales.

Secondly the framework should be directly compatible to the basic form of Newton's Law of Cooling for isothermal wall. The working method should be directly applicable to an isothermal case simply as an extreme end of a general spectrum of non-isothermal cases. Thus, a framework method to be developed should seamlessly work for isothermal cases in exactly the same way as the conventional HTC based method: do not 'fix' something which works, as the conventional HTC has done so extensively and successfully in such conditions. Hence, the framework methodology should also need to be hinged on its direct applicability to an isothermal case. It then becomes apparent that we should have some insightful understanding in order to address the question: how does the conventional HTC work for an isothermal case? Although there have been many papers on the validity of the Newton's law of cooling from the perspective of experimental accuracy, rarely has a discussion been carried out from a theoretical perspective regarding its related underpinning. Therefore, we should take a more fundamental close look into the HTC working for an isothermal wall case, in order to be in a better position to approach developing a new framework and implementation methodology as intended.

The present paper is organised as follows. Firstly, we will take a close and fundamental look at wall bounded convective heat transfer for gaining relevantly useful insights into how the convectional HTC works for an isothermal wall. Then the Spectral Heat Transfer Coefficients (SHTC) will be presented as an extended framework to non-isothermal walls. The more detailed method implementations will be discussed and followed by several computational examples to demonstrate the validity and effectiveness of the present method in 2D and 3D settings of general relevance and interest.

2. Some relevant fundamentals: HTC working for isothermal wall

The aim is to develop a unified framework which is applicable to general non-isothermal walls and also functions in the same way as Newtons' law of cooling for isothermal walls. We need to take a close look at the latter. A general issue of interest is: what are the difference and relation between a global influence and a local performance response? More specifically, q, HTC and T_w are all seemingly local parameters, how do they reflect global influence, if any?

In keeping with Newton's law of cooling, it is assumed that the thermal field is linear. The corresponding situation can be found in an incompressible flow where the energy equation is decoupled from the continuity and momentum equations, and as such the temperature thermal field is passively driven by the velocity (momentum) field, e.g. [23]. For a simpler form of presentation, we express the flow variables in vector $\boldsymbol{U}$. After the flow momentum field is solved independently, $\boldsymbol{U}$ is known. The linear energy equation can be simply expressed as:

$$\frac{\partial T}{\partial t} - L(\boldsymbol{U},\ T) = 0 \tag{2.1}$$

where L denotes a linear operator for temperature T as the variable with the given flow field $\boldsymbol{U}$. Consider a steady state fluid temperature field subject to wall temperature T_w on a solid boundary and a reference temperature T_{ref}. A temperature response $\delta T = T\text{-}\ T_{ref}$ at any point within the 3D fluid domain will be proportional to its originating boundary disturbance over a wall segment of area δA at a wall temperature perturbation $\delta T_w = T_w\ \text{-}\ T_{ref}$.

$$\delta T = C(\boldsymbol{U})\delta T_w \delta A \tag{2.2}$$

where $C(\boldsymbol{U})$ is a spatially varying coefficient dependant only on the already-solved fluid momentum field $\boldsymbol{U}$ and thus is a constant of proportionality between the response δT and its source disturbance δT_w per unit area. The total temperature response to all wall temperature disturbances from the entire solid wall boundary of area A can thus be obtained by summing up the contributing influences from all boundary points (each with its differential area dA) respectively through a boundary integration.

$$\left(T - T_{ref}\right) = \oint_0^A C(\boldsymbol{U})\left(T_w - T_{ref}\right)dA \tag{2.3}$$

The integrand is effectively the local wall temperature disturbance weighted by the spatially variant but T_w invariant coefficient. Differentiate the equation above (Eq. (2.3)) with respect to the wall normal distance n_w, assuming a constant thermal conductivity k. We then have

$$q = \oint_0^A g(U)\left(T_w - T_{ref}\right)dA \tag{2.4}$$

where $g(\boldsymbol{U}) = k\frac{\partial C(U)}{\partial n_w}$. Dimensionally in SI units, $g(\boldsymbol{U})$ has units of $W/m^{-4}K^{-1}$. If one thinks of a link between $g(\boldsymbol{U})$ and HTC, the units can be simply rewritten as $(W/m^2/K)/m^2$. Physically, the term $g(\boldsymbol{U})$ is the influence of a unit wall temperature disturbance per unit wall area (when $(T_w - T_{ref}) = 1$ and $dA = 1$) on heat flux q at a point of interest. Mathematically, $g(\boldsymbol{U})$ is Green's function linking a field response specifically to a boundary perturbation disturbance for a linear system as it is generally defined.

The boundary integration (Eq. (2.4)) means that the total influence on the heat flux at the point of interest needs to be summed up for all differential boundary elements over the entire wall boundary surface A, by superposition for the linear system. As such, $g(\boldsymbol{U})$ can be labelled as a local Influence Coefficient (IC) for a boundary point subject to a non-unit wall temperature disturbance on a non-unit area. We now consider the two types of conditions of primary relevance to the present work.

For an isothermal wall case (T_w = constant everywhere on the entire solid boundary), we then have,

$$q_w = \left(T_w - T_{ref}\right)\oint g(\boldsymbol{U})dA \tag{2.5}$$

The key point is that the boundary integration now depends only on a known momentum field $\boldsymbol{U}$, and is completely independent of the now uniform wall temperature disturbance in this case. We thus can simply denote the boundary integration in Eq. (2.5) over the wall surface as h ($\boldsymbol{U}$):

$$h(\boldsymbol{U}) = \oint g(\boldsymbol{U})dA \tag{2.6}$$

Regardless of how the influence coefficient/Green's function $g(\boldsymbol{U})$ is actually distributed (in a known or unknown form), the most relevant point from Eq. (2.6) is that h or HTC only depends on the given flow field. We then are able to get the standard form of Newton's law of cooling:

$$q_w = h(\boldsymbol{U})\ \left(T_w - T_{ref}\right) \tag{2.7}$$

The physical constraint means that the heat flux needs to diminish when the wall temperature disturbance $(T_w - T_{ref})$ becomes zero. Thus, T_{ref} needs to be the adiabatic wall temperature T_{ad} for the physical consistency.

The key to the above working is that the local wall temperature disturbance is the same for the entire wall boundary. Because of this, the sum of the local influences (the local temperature disturbance weighted by the local influence coefficient) for each and every differential element of the entire wall boundary simply becomes the constant temperature disturbance weighted by the sum of the influence coefficients. From the process of reaching Eq. (2.7), we can conclude that both the flow field and wall temperature disturbances over a wall boundary do have global influences on a local heat flux. Under an isothermal condition, it just so happens that global and local temperature disturbances are now indistinguishable, which enables a simple direct summation of the local influence coefficients/Green's functions, leading to the simple form of the HTC in Newton's law of cooling.

On the other hand, for a non-isothermal wall, the local heat flux at any location of the wall boundary will now have to be explicitly influenced by all locations in terms of summed local wall temperature disturbances weighted by corresponding local influence coefficients (Eq. (2.4)). The equivalent discrete form of the general integral expression (Eq. (2.4)) for the heat flux at point (I,J) on a solid wall boundary with M_w x N_w discrete wall surface elements is:

$$q_{IJ} = \sum_{i=1}^{M_w}\sum_{j=1}^{N_w} g_{IJ}(\boldsymbol{U})_{ij}\Delta T_{ij}\Delta A_{ij} \tag{2.8}$$

where M_w *and* N_w are the numbers of mesh cells in the two wall parallel directions respectively (Fig. 3). $g_{IJ}(\boldsymbol{U})_{ij}$ is the influence coefficient of boundary element (i, j) with regard to the heat flux q_{IJ} of point (I, J). Physically, $g_{IJ}(\boldsymbol{U})_{ij}$ represents the specific influence (per unit temperature disturbance per unit area) from wall boundary mesh element (i, j) of area ΔA_{ij}. Each mesh element will have an influence coefficient (discrete Green's function). Thus if we directly calculate these discrete Green's functions for an non-isothermal case, M_w x N_w solutions will be needed. In contrast, for an isothermal case, only would one calculation be needed for the HTC distribution over the wall surface.

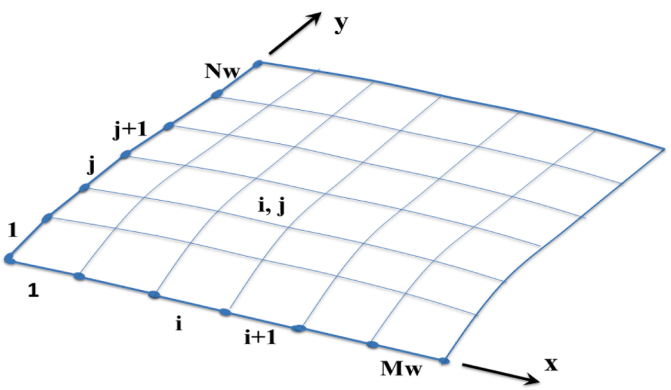

Fig. 3. Discrete wall boundary surface for a 3-D domain.

The insights into the working of Newton's law of cooling for an isothermal wall effectively lead to a method development target. The question then is: can an integral of the kind for the isothermal case also be identified and established for a non-isothermal wall in a principally similar manner?

3. Proposed framework and method: SHTC

3.1. Framework

Given the key requirement of capturing the global influences of the entire wall boundary on any of its local point, it is proposed to harness a spectral approach to achieving this effectively and accurately. A solid wall temperature distribution tends to be smooth, typically much smoother than that in a fluid domain, due to the strong thermal diffusion in solid. Thus, wall temperature is justifiably more amenable to a spectral representation. Consider a general discrete spectral approximation of N_m modes for wall temperature disturbances over a wall surface,

$$\Delta T(x,y) = \sum_{m=1}^{N_m} C_m B_m(x,y) \tag{3.1}$$

where $B_m(x,y)$ is the basis function of the spectrum for mode m, spatially-dependant but wall-temperature independent. C_m is the modal coefficient, effectively the magnitude of temperature disturbance for mode m. More importantly, C_m is spatially-independent. The superpositionality of the linear thermal system means that we can apply the boundary integration to each and every spectral mode separately first and sum them up. Given the spectral modal coefficient C_m ($m = 1, 2, \ldots, N_m$) being spatially invariant, we only need to keep the basis function in the boundary integral. Thus, the local wall heat flux equation (Eq. (2.4)) then becomes:

$$q(x,y) = \sum_{m=1}^{N_m} C_m \oint_0^A g(U) B_m dA \tag{3.2}$$

Denote the boundary integral for mode m as $H_m(x,y) = \oint_0^A g(U) B_m dA$, which is spatially variant, but importantly wall temperature invariant, leading to:

$$q(x,y) = \sum_{m=1}^{N_m} C_m \, H_m \tag{3.3}$$

We now have the intended principal expression for heat flux in terms of the product of the HTC-like H_m and the temperature disturbance-like C_m for spectral mode m. The spectrum can be fixed by N_m solutions. Thus, if N_m is much smaller than the total number of boundary mesh points, we shall get a significant computational advantage as intended. In analogy to the HTC as in Newton's law of cooling, we call H_m 'Spectral Heat Transfer Coefficient' (SHTC).

To determine the value of the SHTC for each mode, we again make use of the linearity to decompose the total flux into N_m components corresponding to N_m modes respectively.

$$q = \sum_{m=1}^{N_m} q_m \tag{3.4}$$

Each mode can be dealt with independently by the mode-balance:

$$q_m = H_m C_m \ , \qquad (m = 1, \ 2, \ \cdots, \ N_m), \tag{3.5}$$

For a given mode m, we can first compute (or experimentally measure) the wall heat flux distribution q_m with a specified wall temperature profile (thus C_m). Then we shall have:

$$H_m = q_m / C_m \qquad (m = 1, \ 2, \ \cdots, \ N_m) \tag{3.6}$$

which is in fact similar to working out the HTC from the computed/measured heat flux q and specified wall temperature disturbance ΔT_w (Eq. (1.1)), $h = q/\Delta T_w$. In the following section, we will also find out how the first base mode of the SHTC can be formulated to correspond exactly to Newton's law of cooling for an isothermal wall.

3.2. Fourier mode balance for SHTC

Fourier spectral methods are shown to be effective in computing temporally and spatially varying flows (e.g. [24–26]), as well as fluid-solid coupled conjugate heat transfer (e.g. [27,28]). In this section, the SHTC methodology will be presented in conjunction with the Fourier spectral method. The methodology will be described here for a 2D plane fluid domain bounded by a solid wall boundary line for simplicity. We will first look at a periodic domain for a full Fourier-series, and then a non-periodic one by making use of a half range Fourier-series ('Fourier Cosine Series'). The detailed formulations for a 3D fluid domain bounded by a solid wall boundary surface will be given in Appendix B. Both 2D and 3D results will be presented in Section 4.

3.2.1. Periodic Fourier series

Consider a 2D fluid domain bounded by a solid wall with a total of M_W mesh elements with a 1D streamwise surface coordinate in the x direction, considering the 2D boundary surface shown in Fig. 3 with a unit length and no variation in the second (y) direction. The wall temperatures are taken at the mesh cell centre points. Assume a spatial periodicity, the wall temperature disturbance distribution over the wall boundary can be represented by a standard Fourier series retaining N_F harmonics. Wall mesh points are indexed by i, and the corresponding spatial locations are marked by angle α_i.

$$\alpha_i = 2\pi i / M_w \ , \qquad (i = 1, \ 2, \ \ldots, \ M_W) \tag{3.7}$$

Wall temperature disturbance ΔT_i for mesh i (subscript 'w' for the wall temperature is omitted for simplicity of presentation for the spectral method) is expressed as,

$$\Delta T_i = \Delta T_0 + \sum_{n=1}^{N_F} (A_n \cos n\alpha_i + B_n \sin n\alpha_i) \tag{3.8}$$

ΔT_0 the zeroth harmonic is the spatial average over the entire boundary, thus a constant base for all points on the wall. The N_F harmonic spectrum is controlled by $2N_F + 1$ parameters, each corresponding to a Fourier mode. Eq. (3.8) can also be expressed as a linear sum of $2N_F + 1$ Fourier modes for the wall temperature disturbance at point i:

$$\Delta T_i = \Delta T_0 + \sum_{n=1}^{N_F} (\Delta T_{An_i} + \Delta T_{Bn_i}) \tag{3.9}$$

Correspondingly heat flux at mesh point i is decomposed to $2N_F + 1$ modes respectively:

$$q_i = q_{0i} + \sum_{n=1}^{N_F} (q_{An_i} + q_{Bn_i}) \tag{3.10}$$

Take a particular note that the heat flux is only decomposed to a mode level as in Eq. (3.10), rather than further approximated by a Fourier spectrum as for the wall temperature (Eq. (3.8)). This is intentional as the wall temperature distribution over a boundary surface tends to be much smoother than the heat flux distribution. Also, technically we will only need to decompose heat flux into modes in order to make use of the superposition.

Superpositionality of different modes means that the disturbance (input) and response (output) for each mode needs to be balanced in its own respectively. Now we make use of the mode balance. Firstly, for the zeroth harmonic, the general heat flux equation (Eq. (2.4)) becomes (noting ΔT_0 is constant over the entire wall boundary)

$$q_{0_i} = \oint g(U)\Delta T_0 dA = \Delta T_0 \oint g(U)dA \tag{3.11}$$

The boundary integral depends only on the flow and is denoted as H_{0_i}, we then have for mesh point i:

$$q_{0_i} = H_{0_i}\Delta T_0 \tag{3.12}$$

Now we see that the zeroth harmonic mode balance is in exactly the same form as Newton's law of cooling, valid for an isothermal wall, as intended.

Next, consider the Fourier mode balance for the nth harmonic of two components. For the cosine term, given that A_n, the coefficient (magnitude) of temperature disturbance, is constant over the entire wall boundary, we have

$$q_{An_i} = \oint g(U)\Delta T_{An} dA = A_n(\oint g(U)cos n\alpha dA) \tag{3.13}$$

Note also that the boundary integral $(\oint g(U)cos n\alpha dA)$ depends only on the flow and the spatially variant but known basis function. We thus denote the boundary integral as H_{An_i}, then we have for mesh point i:

$$q_{An_i} = H_{An_i}A_n \tag{3.14a}$$

Following the mode balance procedure similarly for the sine component, we have

$$q_{Bn_i} = H_{Bn_i}B_n \tag{3.14b}$$

Therefore, we can represent the local flux at point i in form of a sum of $2N_F+1$ terms of corresponding Fourier spectral modes:

$$q_i = H_{0_i}\Delta T_0 + \sum_{n=1}^{N_F}(H_{An_i}A_n + H_{Bn_i}B_n) \tag{3.15}$$

It means that if we use the spectrum to construct heat flux for any given non-isothermal wall temperature distributions as we use HTC for q with Newton's law of cooling for an isothermal wall, we need to determine the $2N_F+1$ SHTCs.

It is useful to be reminded that the first term (zeroth harmonic) corresponds to the isothermal condition as in Newton's law of cooling. All terms share the common feature that the proportionality coefficients are local, but the temperature disturbances (in terms of either the base average wall temperature disturbance or the magnitudes of all harmonic coefficients) are all global. Thus we are able to globally set influences in a range of length scales, as intended.

3.2.2. Half-range non-periodic Fourier series

The standard Fourier series is applicable to periodic problems. A non-periodic distribution can however be viewed as one half of a periodic one with the other half being simply mirrored symmetrically (He [29]). In a recent effort in implementing a Chebyshev spectrum for a non-periodic spectral mapping (Chen and He [30]), it appears that the half-range Fourier Series is actually equivalent to a Chebyshev spectrum (as clarified with the derivation in Appendix A). Given this and based on the previous experience, the present author favours treating both periodic and non-periodic problems all under a unified Fourier spectrum, while the latter is easily taken as an option of the same method for a reduced domain.

The half-range Fourier series does have some tangible advantages. The symmetry for the mirrored full period distribution means that only those cosine terms are present, thus it is also called the cosine, or the even-functions Fourier series. In the context of our SHTC methodology, the corresponding Fourier spectrum for the wall temperature disturbances becomes:

$$\Delta T_i = \Delta T_0 + \sum_{n=1}^{N_F} A_n \cos n\alpha_i \tag{3.16}$$

Consequently, we will only need N_F+1 parameters to determine. Correspondingly we follow the same analysis for the SHTC by keeping only the cosine terms. Then we will have the heat flux for mesh point i as:

$$q_i = H_{0_i}\Delta T_0 + \sum_{n=1}^{N_F} H_{An_i}A_n \tag{3.17}$$

Therefore, only do we need N_F+1 SHTCs to be determined if we use this spectral option to construct a local heat flux. Compared to the full periodic spectrum, this is a nearly 50% reduction in the number of solutions required.

The above formulations are presented for a 2D fluid domain bounded by a wall boundary line. The same framework and principal procedure are applicable for 3D cases with a 2D boundary surface. A double Fourier series will be adopted for 3D cases with detailed formulations provided in Appendix B. It is worth noting however that for a 3D case, a cosine Fourier series for a non-periodic domain in the two wall-parallel directions will lead to a reduction in the number of solutions required by a factor of 4, which is quite significant.

3.3. Working procedure

The methodology has been implemented in conjunction with a 3D Compressible Navier-Stokes CFD solver developed, validated and applied by the author and his colleagues for various problems and test cases documented in many publications over more than 30 years.

In relation to the SHTC working procedures, we have two parts. The first is how to generate the SHTC. This is prerequisite regardless of applications. The second part to be discussed is about a common application scenario of using the generated SHTC as boundary condition in solving the conduction equation for a temperature field of a solid-domain.

3.3.1. Generation of SHTC (fluid-domain only)

Given the fundamental assumption of a linear thermal field, each of the multiple spectral modes of boundary disturbances can be completely separately processed and the effects can be superimposed. For a Fourier spectrum with N_F harmonics, we process each of the $2N_F+1$ modes independently. Note that the disturbances of these modes are all global covering the entire wall boundary. A CFD solution for any specified mode will enable to determine the weighting coefficient in the form of SHTC for the mode and for the given flow field. so that we will be able to reconstruct local heat fluxes for any other wall temperature distributions.

For the low speed flow test cases considered, the inlet stagnation temperature T_{01} is taken as the reference fluid temperature T_{ref}, shown to be a good approximation of the adiabatic wall temperature. The magnitude of the temperature disturbance (T_w-T_{01}) should be small enough so that the temperature response will be well within a linear regime even when we solve nonlinear compressible flow equations, but also large enough so that the physical responses are much larger than computer machine errors (or experimental noise). In the present work, temperature disturbances of 3–5% are judged to be sufficiently adequate.

Because of the linear superpositionality, the SHTC for different modes can be generated completely separately in principle and in practice. As a matter of fact, we can run $2N_F+1$ CFD solutions in parallel in different computer cores with a serial CFD code, as the author has done.

More specifically, we consider how the SHTC generation process will proceed in terms of specified wall temperature disturbances for mesh point i ($i = 1, 2, \ldots, M_w$) for a wall boundary with M_w points, as follows.

i) For the zeroth harmonic (the overall average 'isothermal' mode): Specify a constant $\Delta T_0 = (T_w\text{-}T_{01})$ and solve q_{0_i}; Postprocess $H_{0_i} = q_{0i}/\Delta T_0$.

ii) For the nth harmonic (two modes):
   a) Cosine mode: Specify $\Delta T_{Ani} = A_n \cos(n\alpha_i)$ and solve q_{Ani}; Post-process $H_{Ani} = q_{Ani} / A_n$
   b) Sine mode: Specify $\Delta T_{Bni} = B_n \sin(n\alpha_j)$ and solve q_{Bni}; Postprocess $H_{Bni} = q_{Bni} / B_n$

The corresponding solution process for creating the SHTC in a fluid domain with specified wall temperature spectral profiles is charted in Fig. 4.

3.3.2. *Conduction solution with SHTC (solid-domain only)*

In terms of applications, SHTC can be used in various ways similarly to the conventional HTC. An example is the internal cooling or heating designs for thermal management of a fluid-solid coupled system. A common requirement in such cases is to predict the solid domain temperature field for a given flow field. Although a fluid-solid coupled conjugate heat transfer (CHT) calculation can be carried out, a solid-domain-only calculation with a given set of SHTC (similar to a given HTC) would be much more efficient, particularly in a design analysis needing a large number of evaluations.

Given the way SHTCs are generated in the fluid-domain-only setting at different combined forms/'wave shapes' of wall temperature distributions, SHTCs effectively serve to decouple a fluid-solid coupled CHT system. If SHTCs generated are sufficiently accurate, they should be able to be effectively used to reconstruct a coupled CHT solution by serving as boundary condition for a solid-conduction solution in a setting with only a solid-domain. And this seemingly decoupled solution procedure has also been implemented and tested in the present work.

An extra enabler for this SHTC-solid solution is a spatial Fourier transform for the wall-temperature. Again, consider a 2D solid domain with a wall boundary of M_w mesh points (Fig. 3). During the solution we need to apply the convective boundary condition for all mesh points at the wall boundary line. For the given SHTCs and fluid reference temperature, we need to specify the heat flux (Neumann) boundary condition for the solid temperature field. And the heat flux needs to be updated at each iteration step.

More specifically at each iteration of the present explicit time-marching method for the solid conduction solution, we first update the interior temperature field. Then by using the same wall-normal gradient from interior solved points we extrapolate from the two adjacent mesh cell-centre points to get the wall temperatures T_w.

$$T_w = 1.5T_{w+1} - 0.5T_{w+2} \tag{3.18}$$

The temperature disturbance based on the extrapolated wall temperature ($\Delta T = T_w - T_{ref}$) will then be used for the Fourier transform

$$\Delta T_0 = \frac{1}{M_w}\sum_{i=1}^{M_w} \Delta T_i \tag{3.19}$$

$$A_n = \frac{2}{M_w}\sum_{i=1}^{M_w} \Delta T_i cos(n\alpha_i), (n = 1,\ 2, \ldots,\ N_F) \tag{3.20}$$

$$B_n = \frac{2}{M_w}\sum_{i=1}^{M_w} \Delta T_i \sin(n\alpha_i), (n = 1,\ 2, \ldots,\ N_F) \tag{3.21}$$

Eqs. (3.19), (3.20) and (3.21) give the modal amplitudes (all spatially invariant) for the $2N_F + 1$ modes of the wall temperatures. With these global wall temperature shape parameters and the given SHTCs, we can then construct to update the wall heat fluxes for all mesh points on the boundary (Eq. (3.17)) at each iteration during the solid conduction solution.

It should be added that for the half-range Fourier series, all the sine terms will disappear. The corresponding number of spectral modes will be reduced to $N_F + 1$ with only Eqs. (3.19) and (3.20) being needed in updating the wall temperature spectral representation during the solution. The corresponding flow-chart for carrying out the wall temperature Fourier transform and setting the wall heat flux boundary condition with the SHTC for a solid domain solution is given in Fig. 5.

4. Case studies for support

Computations are carried out principally for concept-proof purposes.

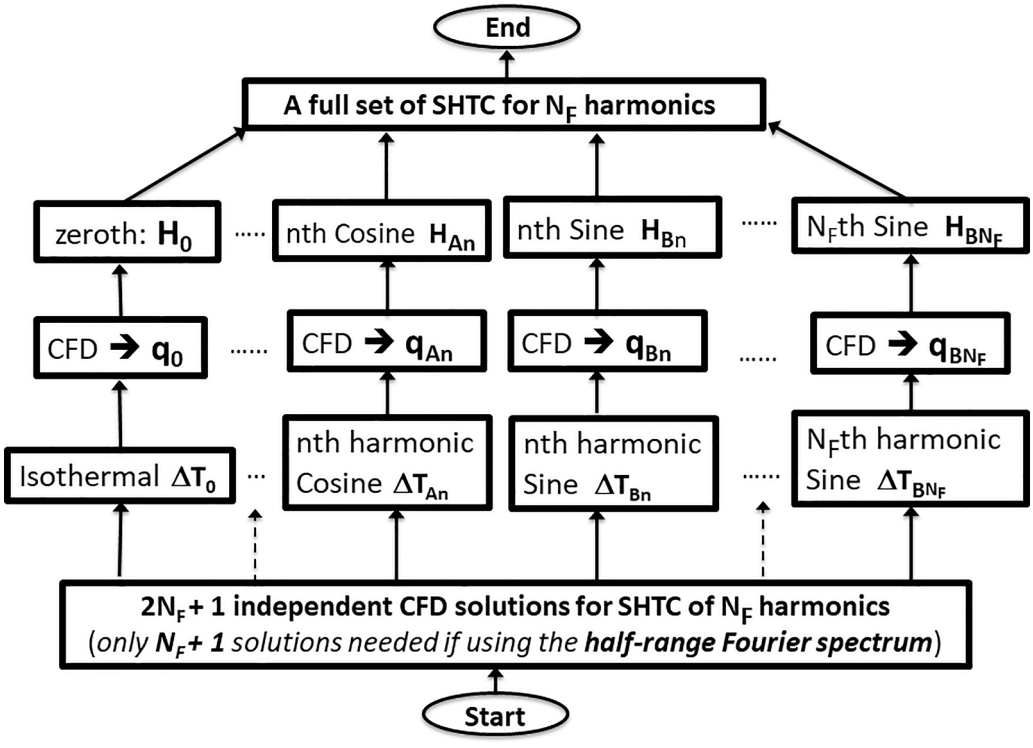

Fig. 4. Parallel Workflow of Multiple CFD runs for generating SHTC.

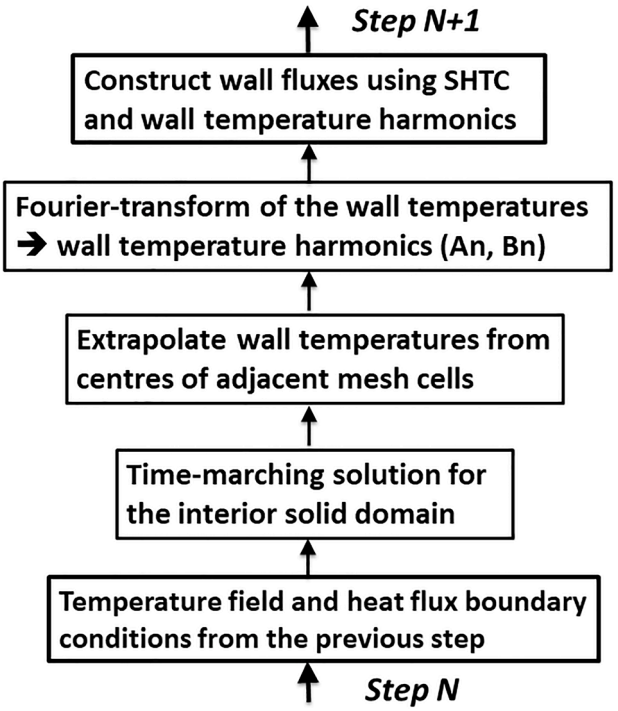

Fig. 5. Flowchart of iteration stepping for solid-domain solution with SHTC.

Some specific aims are:

i) To examine the validity and accuracy of SHTC generation in a decoupled fluid-domain;
ii) To examine the sensitivity to number of spectral modes retained;
iii) To examine the capability and accuracy of the fluid-domain-only generated SHTC in predicting the CHT coupling in a solid-domain-only setting;
iv) To examine the effectiveness of the half-range Fourier SHTC for nonperiodic, as well as for periodic wall temperature distributions;
v) To test and demonstrate the methodology and implementation for 3-D cases.

4.1. Generating SHTC (Fluid-domain only)

For a flat plat laminar boundary layer (Re=1000), a fluid domain consists of a small inviscid inlet sub-domain of 200 × 41 points followed by the wall bounded main flow sub-domain with 200 × 200 mesh. We test the half-range Fourier series with only cosine terms to generate SHTC. For N_F harmonics we thus only need $N_F + 1$ CFD runs for the $N_F + 1$ globally specified cosine wall temperature profiles respectively. The corresponding calculated wall heat fluxes on all mesh points of the wall boundary and the input known coefficients (magnitudes) of the cosine wall temperature profiles for the $N_F + 1$ modes will simply provide the SHTC for all M_w mesh points on the wall boundary:

$$H_i = H_{0i} + \sum_{n=1}^{N_F} H_{Ani}, (i = 1,\ 2,\ \ldots\ldots,\ M_w) \tag{4.1}$$

The basic concept-proof of the SHTC can be shown by using the generated SHTCs for different and un-sinusoidal wall temperature distributions. We compare the wall heat-fluxes directly computed by the CFD, with those constructed through the SHTC based on the Fourier transformed wall temperatures for the $N_F + 1$ modes. We also examine the sensitivity of the spectral representation to the number of modes (harmonics), which is a closely relevant issue for spectral methods in general.

It should be commented that for examining the validity of any wall temperature 'invariant descriptors' (e.g. HTC, SHTC or full discrete Green's functions), it is important to test the wall heat flux construction by using some wall temperature profiles very different from those which are used to generate the 'invariant descriptors' in the first place. This is due to the simple fact that the construction of the total heat flux or each of linearly summed components all follows a same general form of a temperature difference weighted by the descriptor/influence coefficient. Hence the sensitivity and errors of the descriptor may only show up adequately in the constructed heat fluxes if sufficiently different temperature disturbances are provided. The earlier discussion around Fig. 2 shows just how a linearity-led superpositionality may indicate a seemingly strong scalability for the heat fluxes calculated by reconstruction. But the HTC obtained in that case is only valid for the same wall temperature profile, thus is a poor descriptor. Therefore, it seems imperative that we have to test the SHTC generated with the group of sinusoidal wall temperature profiles in completely different wall temperature conditions, as presented and discussed in the following.

First, we examine a streamwise non-periodic wall temperature profile. Fig. 6 shows the mode/harmonic sensitivity of the spectral approximation for the heat flux distribution along the plate, which is the viscous wall. The flux is nondimensionalised by $q_{ref} = T_{01}k_f/L$ with the inlet flow stagnation temperature T_{01}, the inlet fluid thermal conductivity k_f and the plate length L. Fig. 7 shows the specified and spectrally constructed wall temperature differences normalised by the inlet stagnation temperature. The spectral representation is shown to converge very quickly with the number of harmonics/modes. We aim for the required number of modes to be one order of magnitude smaller than the number of wall boundary mesh points (200 in this case). We can see that 10 modes are shown to be sufficient for a practically mode-independent heat flux prediction. A higher number of modes will only result in a very minor improvement. Also shown in Figs. 6 and 7 are the target references: the directly computed heat fluxes and the directly specified wall temperature distributions. Good comparisons between the targets and the spectral approximations are clearly demonstrated.

Given the reduced number of modes (thus flow solutions) required for generating SHTC when the half-range Fourier series option is used, it is of interest to see how the option performs for a periodic case. In practical applications, it may not always be easy, nor desirable, to predetermine if the wall-temperature distributions will be periodic or not, particularly when the wall temperatures are part of the solution for a fluid-solid coupled system. It will therefore be preferable that we use a unified method option without needing to make the periodicity assumption.

We thus consider a spatially periodic trapezoidal wall temperature profile to be spectrally approximated with the half-range Fourier series. Fig. 8 shows the mode/harmonic sensitivity for the heat fluxes, Fig. 9 shows the corresponding results for the wall temperatures. Both show

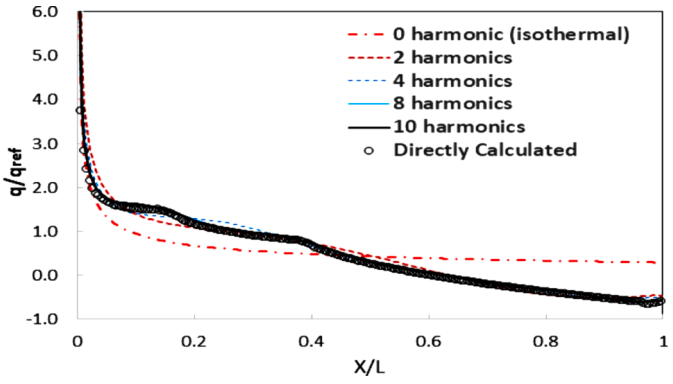

Fig. 6. Harmonic sensitivity of heat fluxes (non-periodic Tw profile).

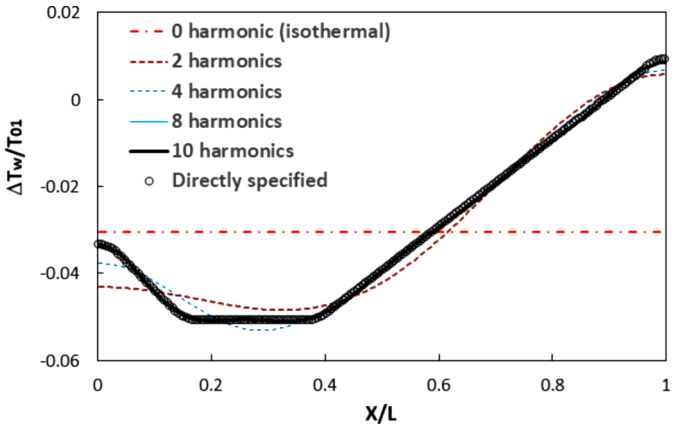

Fig. 7. Harmonic sensitivity of wall temperature (non-periodic Tw profile).

rapid mode/harmonic convergence and the results with 10 harmonics are shown in satisfactory agreement with the directly computed heat fluxes (Fig. 8) and the directly specified periodic but non-sinusoidal target wall temperature distribution (Fig. 9).

4.2. Solid-domain SHTC solution vs. fully coupled CHT

For convective heat transfer, a common application scenario is to predict the temperature field of a solid domain. This is also how Newton's law of cooling with given HTC and T_f is commonly used as boundary condition for a solution to the conduction equation in a solid-domain-only setting. We would thus like to examine if the SHTC may play the same role as the conventional HTC but with a much improved accuracy for a non-isothermal solid domain. The reference target is a fluid-solid coupled conjugate heat transfer (CHT) solution.

Some observational comments should be made here first. In the context of a coupled CHT solution, a question would naturally arise: how can the SHTC generated in a fluid-only setting possibly capture any coupling interference between the fluid domain and an absent solid domain? The question may also be translated to: what do the SHTC actually mean or represent?

Fundamentally, the proportional relation between heat flux and wall temperature difference as in Newton's law of cooling effectively makes the proportionality coefficient HTC act as a transfer function between the two. Clearly this wall temperature-flux transfer function relation is established completely for flow convection in a fluid-domain-only setting as Newton's law of cooling is meant to be. On the other hand, we should also be reminded that for a fluid-solid coupled conjugate heat transfer system, there is a basic physical constraint for the temperature and flux continuity across the fluid-solid interface, as articulated by Perelman [31]. It follows then that the temperature-flux transfer function on the wall boundary established in a fluid-only setting, should be equally applicable to the solid side of the boundary for the solid domain, if the two domains are coupled. Therefore, the wall temperature-heat flux relation in the solid domain is expected to behave the same way (in the same proportionality) as that established in the fluid-domain-only setting. It can thus be argued coherently in the present work that there should be a continuity of the temperature-heat flux transfer function across the fluid-solid interface (regardless of which side of the interface the transfer function is originated initially).

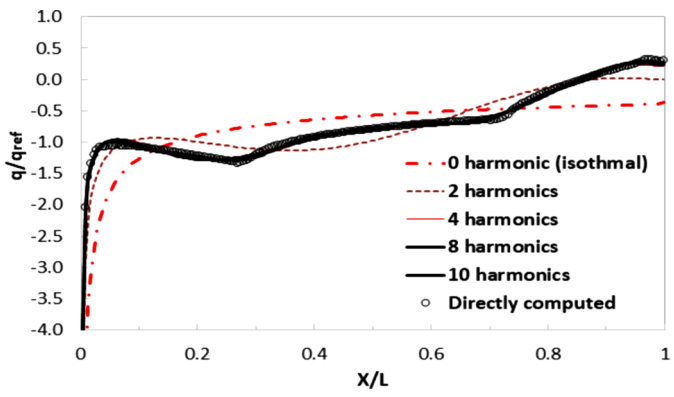

Fig. 8. Harmonic sensitivity of heat fluxes (periodic Tw profile).

For the present case, multiple terms of SHTC can be simply regarded as multiple transfer functions. The same reasoning for the standard HTC as a single value transfer function should apply for each and every mode of the spectrum, based on superpositionality. As a matter of fact, the equality of a wall temperature-flux transfer function across a fluid-solid interface was used effectively by He and Oldfield [32] and He [27]. In these previous works, a transfer function established in a solid-domain only setting for transient heat transfer experiments (Schultz and Jones, [33]) was effectively applied also to the fluid side in formulating a semi-analytical unsteady CHT interface method. For the present work, the SHTC generated in a fluid-only setting as a set of transfer functions should thus equally dictate how the temperature disturbance and heat flux are correlated in proportion on the wall boundary of the solid-domain-only setting. Given the same reference fluid temperature, a solid domain with the SHTC as the boundary condition should in principle produce a solution directly comparable to a target fluid-solid coupled CHT solution.

To verify the validity, accuracy and effectiveness of the SHTC method in this regard, a comparative case study is set up. Two calculations are compared. The first is a fully coupled CHT solution with a computational domain setup as shown in Fig. 10. The fluid domain configuration and inflow conditions are the same as in the previous fluid-domain-only setting, presented in Section 4.1 (flat plate laminar boundary layer of Re=1000). A solid domain is now added directly interfacing with the fluid wall boundary. The solid material is stainless steel with density 8000 kg/m3, specific heat capacity 500 J/kg/K, and thermal conductivity 15.7 W/m/K. At the bottom side of the solid domain, a constant cooling heat flux of $q/q_{ref} = 3.5$ ($q_{ref}=T_{01}\ k_f / L$) is applied between 60% and 70% plate length. Other parts of the bottom wall and side walls of the solid are subject to an adiabatic condition. Hence, the wall temperature distributions will be completely different from those used for generating the SHTC in Section 4.1. The second calculation is carried out for the solid-domain-only setup. In this case, the solid-domain top boundary will be subject to the boundary condition with the SHTC generated with the half-range Fourier spectrum. The inlet stagnation temperature is also taken as the reference fluid temperature. Both the CHT and solid-domain-only cases are subject to the same specified heat flux patch at the bottom boundary of the solid domain.

Fig. 11 shows the temperatures contours of the two solutions. For the CHT solution (Fig. 11a), the contours in the fluid domain are in the stagnation temperature. We can see a clear tendency that the temperature contour lines are biased toward downstream once reaching the fluid side (Fig. 11a), which is expected due to the dominant convection in the fluid domain. On the other hand, in the solid domain, the temperature disturbances are diffused largely equally in all directions, manifested by the symmetrical contour pattern in the up- and down-stream directions. The overall good agreement in temperatures between the solid-domain-only solution with the SHTC (Fig. 11b) and the solid part of the fully coupled CHT solution (Fig. 11a) is clearly achieved.

Now we look at more detailed comparisons between different solutions. Fig. 12 shows the heat flux distributions at the fluid-solid interface for the CHT solution (Fig. 11a) which is also the top boundary for the solid-domain-only solution (Fig. 11b). Fig. 13 shows the comparison in the corresponding calculated wall temperatures. Here in addition to the CHT solution as the target reference, three solid-domain-only solutions are included for comparison. The two SHTC solutions with 10 harmonics and 20 harmonics respectively are included to indicate the mode/

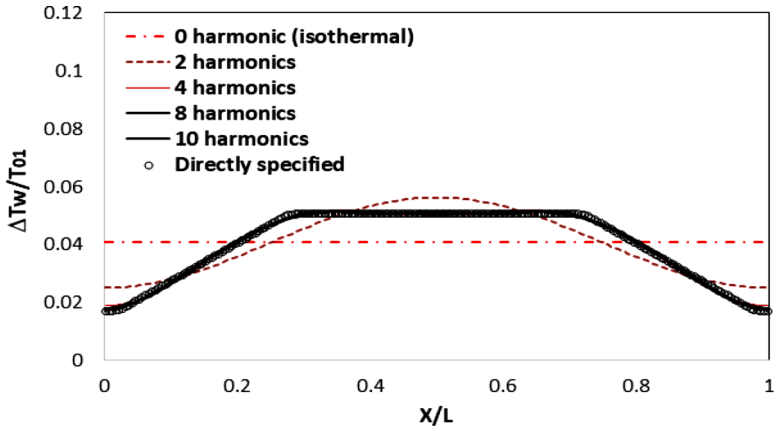

Fig. 9. Harmonic sensitivity of wall temperatures (periodic T_w profile).

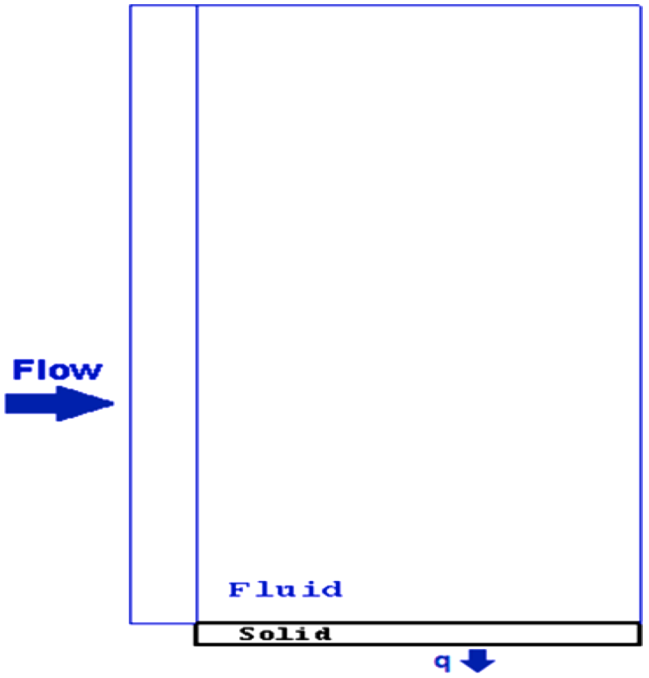

Fig. 10. Fluid-solid coupled domain for target reference CHT solution.

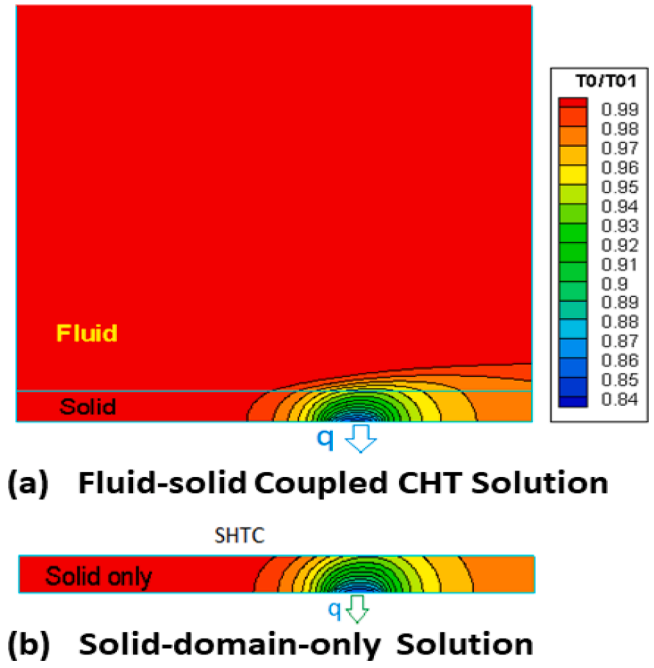

Fig. 11. Temperature field comparison between CHT and solid-SHTC solutions.

harmonic convergence.

Additional to the two solid solutions with the SHTCs, a third solid-domain solution with only the zeroth harmonic mode SHTC is also included. It must be noted that for this third solid-domain solution, the temperature difference used in constructing the local heat flux is specifically taken to be the local temperature difference, rather than the overall spatial average temperature difference as the zeroth harmonic mode of the SHTC is supposed to be. This third solid-domain solution using the local temperature difference is in fact the same as that commonly adopted in the standard form of Newton's law of cooling, it is thus labelled as 'Isothermal HTC with local ΔT_w' in the result comparisons presented in the figures. It is very clear that the conventional HTC based solution can lead to significant errors when used in this non-isothermal case. The maximum errors for the present case are about 35% for the heat flux (Fig. 12), and about 75% for the wall temperature (Fig. 13). These levels of errors are most likely to be regarded as unacceptably high for many applications.

All the results clearly and consistently demonstrate that the present SHTC method leads to a qualitatively marked improvement over the conventional HTC based prediction. The question of whether or not the

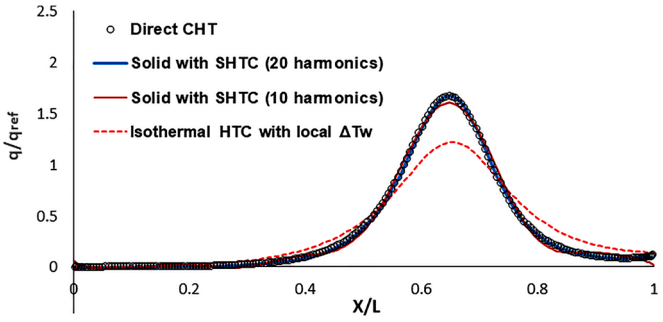

Fig. 12. Comparison of wall heat fluxes computed by different models.

SHTC created in a fluid-only setting can properly capture the fluid-solid coupling is answered positively and definitively.

It should be highlighted that the SHTC results show a good harmonic/mode convergence. Be reminded that in these cases, the number of harmonics is almost the same as the number of modes, as only the

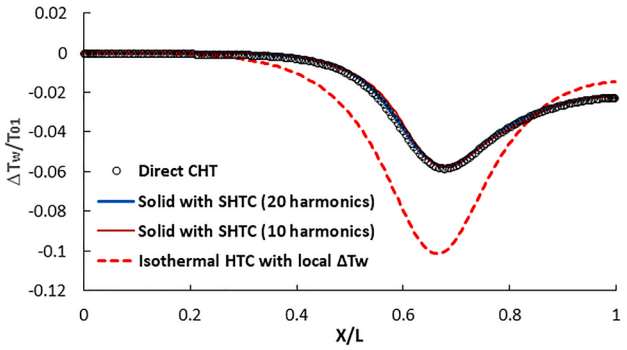

Fig. 13. Comparison of wall temperatures computed by different models.

half-range Fourier-series is used. For the present case of 200 mesh points over the solid wall boundary (the interface for the CHT), we see that the SHTC solution with 20 harmonic modes (requiring 21 CFD solutions for generating the SHTC) leads to an excellent agreement. In fact, the SHTC solution with only 10 harmonics (requiting 11 CFD solutions), gives a quite satisfactory comparison with the target CHT solutions (Figs. 12, 13). Hence for 2D cases, we are able to make an order of magnitude reduction in number of required CFD solutions in comparison to a direct method of solving the influence coefficients/Green's functions. For 3D cases, the SHTC solutions should correspondingly be expected to lead to a reduction in number of CFD solutions by two orders of magnitude, as will be shown next.

4.3. Three dimensional cases

The 2D cases presented above serve well as a concept-proof for the SHTC framework and principal methodology. The same procedure is applicable to 3D cases. The main difference is that a double Fourier series in the two wall-parallel directions (Fig. 3) will be used for 3D cases with the detailed formulations presented in Appendix B.

To validate the implementation and demonstrate the 3D application potential, we consider an annulus sector configuration with an outer fluid layer and an inner solid layer (Fig. 14a). The flow is laminar subject to a uniform axial inlet flow (Re=1000 based on the axial domain length). The outer boundary of the fluid domain is subject to an inviscid wall and the inner boundary is a viscous wall interfacing with the solid domain. The solid material is the same stainless steel as that used in the 2D cases. The numbers of mesh points for the fluid domain are 100, 100 and 60 in the axial, tangential and radial directions respectively. The corresponding ones for the solid domain are 100, 100, and 40 respectively, with the mesh density indicated in the close-up view of the computational domain (Fig. 14b). The wall boundary/interface surface is thus covered by $M_w x N_w$=100 × 100 mesh cells, as indicated in Fig. 3.

The mesh spacing of the fluid domain is refined towards the wall to resolve the boundary layer as usual. Attention is also drawn to the streamwise mesh spacing distribution, also refined towards the inlet in the near wall region (as indicated in the closeup, Fig. 14b). Hence the mesh on the wall surface is non-uniformly spaced as normally the case in practical applications. It is relevant to note that for a discrete Fourier spectral representation, a very useful and fundamental property is the orthogonality between different modes. The mode orthogonality requires the interval of the sample points in the angular space to be uniform, and this requirement can be easily met when implemented accordingly for 2D (Eq. (3.7)) and 3D (Eqs. (A.9) and (A.10), Appendix B) cases regardless of the wall-mesh spacing distributions.

In terms of the 3D cases, we first consider the fluid-domain-only setting for generating the STHC following the working procedure as described in Section 3.3.1. Take a non-periodic distribution as one half period approximated by the half-range Fourier spectrum in each of the two wall-parallel directions respectively. We then need to retain only the cosine x cosine terms in the double-Fourier series (Appendix B). The corresponding number of SHTC modes will be $(M_F+1)(N_F+1)$ when we retain M_F harmonics in the x direction and N_F harmonics in the y direction respectively (Fig. 3). Thus for the present case with 100 × 100 wall surface mesh points, a motivational consideration as stated in the introduction is to see if we can establish an adequately accurate SHTC set with the number of harmonics (modes) smaller than 10 in each direction, so that the total number of CFD solutions needed will be in the order of, or smaller than 10 × 10. In the present case, we take 6 harmonic modes in each of the two wall-parallel directions respectively. In total, 49 CFD solutions are run for generating the corresponding set of SHTC. The base zeroth harmonic mode is for the overall averaged temperature disturbance over the entire wall boundary, corresponding to an isothermal condition. Thus, the SHTC term for the base zeroth harmonic is also denoted as 'Isothermal HTC' as for the 2D test cases presented earlier.

Having generated the SHTC set with 6 × 6 harmonics (7 × 7 modes), we now are in the position to perform the solid-domain-only calculations for different and unknown wall temperature distributions under different thermal boundary conditions. Consider two local heating conditions for the inner wall boundary of the solid domain. The first one is subject to a heating patch of q/q_{ref}=3.5 located between 20% and 40% streamwise length and 20%–40% span on the inner boundary surface of the solid domain, labelled as 'frontal heating'. In the second case, the heating patch of the same size is placed at the middle of the inner boundary surface on top of a constant base heat flux of q/q_{ref} = 0.35 applied to the entire inner boundary surface, denoted as 'middle heating'. The heating patch on the bottom inner boundary of the solid domain can be seen from the bottom surface view in Fig. 14. It is worth noting that even when the heating is applied in a very non-smooth fashion (a constant heat flux applied on the small square area of the

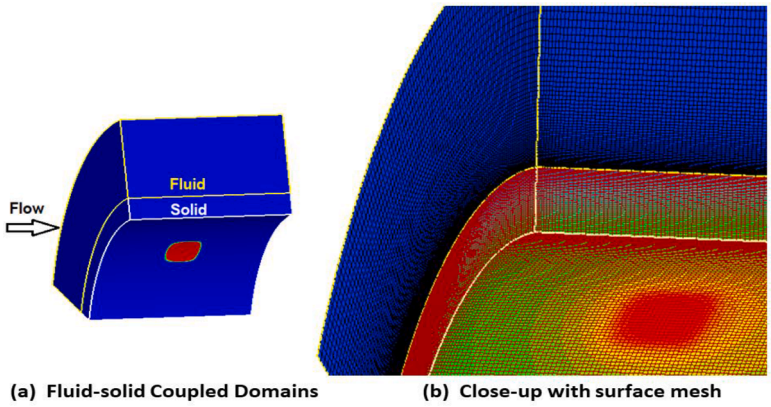

Fig. 14. 3-D annular fluid-solid coupled configuration.

inner surface), the solid temperatures still look quite smooth even around the heating area, due to the very strong local thermal diffusion in solid.

The temperature distributions on the top surface (wall boundary/interface) of the solid domain can be seen in Fig. 15 for the frontal heating case. Three solutions are compared: the fluid-solid coupled conjugate heat transfer (CHT, Fig. 15a), the solid-domain solution with the present SHTC of 6 × 6 harmonics (Fig. 15b) and the solid-domain solution with the zeroth harmonic mode SHTC and local temperature difference, which effectively is in the standard form of Newton's law of cooling, denoted as 'Isothermal HTC with local ΔT_w' (Fig. 15c).

We can see that for the 3D configuration, the new SHTC as the boundary condition for a solid-domain-only (Fig. 15b) captures quite accurately the fluid-solid thermal coupling in good agreement with the fully coupled CHT solution (Fig. 15a). The conventional use of the HTC certainly leads to noticeable differences (Fig. 15c). More detailed comparisons of the streamwise wall temperature distributions are taken on an axial cut-plane through the middle of the heating patch, as shown in Fig. 16. While the SHTC and CHT solutions are in good agreement, the discrepancies between the conventional HTC solution and the reference target CHT solution are up to 15–20%, higher towards the downstream locations, attributable to the accumulated convective temperature 'history effect' (He [23]).

For the second case of the heating patch at the middle in addition to a constant base flux heating on the bottom boundary, Fig. 17 shows the top surface view of the temperature contours of the solid domain. Again, we see that the same set of the SHTC generated for a specified set of simple sinusoidal wall temperature profiles can produce a very good solid temperature solution in comparison with the target fully coupled CHT solution for completely different thermal boundary conditions. In this case, the differences between the conventional HTC based method (Fig. 16c) and the reference CHT solution are larger. This may be attributed to two different aspects of the temperature 'history effect'. Firstly, the base constant flux heating over the whole bottom boundary surface should have a larger accumulated convective 'history effect' on the peak temperature region at a more downstream location as in this case. An additional factor may be due to the difference in the thermal disturbance propagation between a fluid domain and a solid one. The travelling of temperature disturbances in a fluid domain will be largely convective, thus markedly directional from upstream to downstream as a convection is meant to be. In a solid domain however, the disturbances only travel by diffusion and thus to both flow upstream and downstream directions equally. When the fluid and solid domains are coupled, the solid domain provides a distinctive extra path for temperature disturbances to influence upstream by changing the wall temperature in an upstream region through the strong thermal diffusion in solid (He [23]). This distinctive fluid-solid coupling effect is well captured by the SHTC.

Fig. 18 shows the streamwise wall temperature distributions taken on an axial cut-plane through the middle of the heating patch. The streamwise error distribution of the conventional HTC based calculation ('Isothermal HTC with local ΔTw' vs. 'CHT' in Fig 18) for this middle

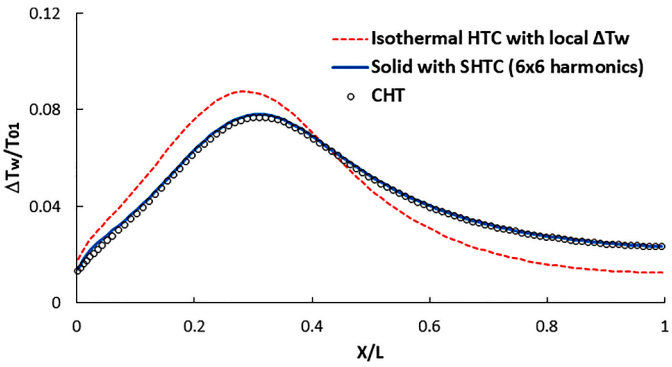

Fig. 16. Streamwise wall temperature distributions computed by different models (taken from an axial cut-plane through the middle point of the heating patch).

domain heating case can be usefully compared to that for the frontal heating case (Fig. 16). The middle heating case shows a stronger 'history effect' manifested in consistently higher overpredicted wall temperatures by the conventional HTC based solution for the whole streamwise boundary surface length, as well as higher peak errors (about 25–30%, as shown in Fig. 18), compared to the frontal heating case (Fig. 16).

Overall, the computational results presented and discussed above for the 2D and 3D cases all serve very well as a strong concept-proof of the present SHTC method and are clearly indicative of its application potential. More specifically, the present 3D cases do demonstrate that the proposed Spectral Heat Transfer Coefficient approach can indeed reduce the number of CFD solutions required by two orders of magnitude compared to a direct method of solving the influence coefficients/Green's functions.

5. Concluding remarks

It has long been recognised that Newton's law of cooling works well for isothermal walls as in the condition at which Newton first tested and established the simple proportional relation for heat flux and temperature difference: $q \propto (T_{wall} - T_{ambient})$. However, its applicability to non-isothermal walls can be regarded as varying from being uncertain to very poor. A full description with local influence coefficients/Green's functions is generally difficult and costly to implement, chiefly caused by the locality of Green's functions: relating a local disturbance to a local response. In considering a possible alternative framework and working method, we would like to first ask some seemingly simple questions: why should Newton's law of cooling work for an isothermal wall (or what is the corresponding theoretical underpinning)? More specifically, what does T_{wall} mean, a local or global disturburbance? And what does the proportionality (HTC as we know it) represent: a local or global influence?

A close look at a linear thermal system for wall bounded flow clearly indicates that T_{wall} and HTC represent global disturbances and global

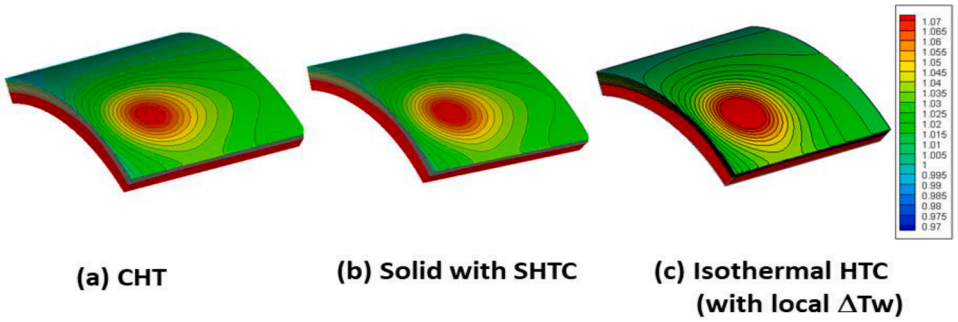

Fig. 15. Wall surface temperature contours computed by different models ('frontal heating').

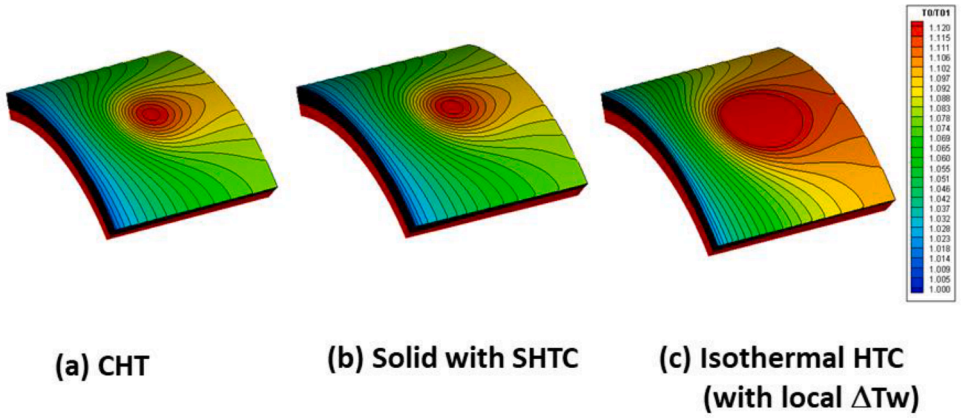

Fig. 17. Wall surface temperature contours computed by different models ('middle heating').

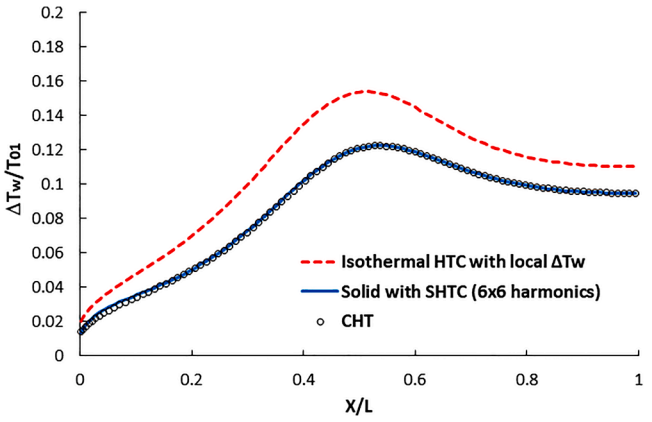

Fig. 18. Streamwise wall temperature distributions computed by different models (taken from an axial cut-plane through the middle point of the middle heating patch).

influences respectively. The simple form of Newton's law of cooling is theoretically hinged on the spatially invariant temperature disturbance as in an isothermal wall setting. The myth of the HTC working in this case seems to be rooted in global and local wall temperature disturbances becoming indistinguishable for an isothermal wall.

In contrast to solving the local-local influence-response as in a direct Green's function approach limited by the locality, it is proposed that the new method should instead approach the problem globally. The wall temperature disturbances can be set globally, starting from a long length-scale for the whole domain, refined systematically and efficiently to shorter but still mesh-resolvable scales. In addition, it is also intended that the framework formulation and working method should be usefully reduced to exactly the same form as Newton's law of cooling for an isothermal case. As such we shall have a unified framework and working method applicable to both non-isothermal wall and isothermal wall cases. The latter can simply be regarded as a temperature disturbance of an infinite length-scale.

Given the background and motivational considerations, a framework is proposed centred around 'Spectral Heat Transfer Coefficient' (SHTC). Wall temperature disturbances, being much smoother by the much stronger thermal diffusion in solid than those in fluid, are naturally suited for a spectral modelling accurately and effectively with only a small number of spectral modes. Each SHTC term corresponding to one spectral mode can be worked out simply and independently given the superpositionality.

The framework is implemented in a Fourier spectral method, and the SHTC can be obtained by a harmonic mode balance in a straightforward way. The baseline full-range Fourier series is for a spatially periodic wall temperature distribution. It is also shown very usefully that a half-range Fourier series model is directly equivalent to a Chebyshev spectral method. Thus, the present Fourier method is applicable to both periodic and non-periodic wall temperature distributions.

The corresponding working procedure and formulations in both 2D and 3D settings are presented. Computational examples for both 2D and 3D cases clearly and consistently demonstrate the validity and effectiveness of the proposed framework and working method implementation.

It should be commented that although the present work approaches the problem computationally, the proposed SHTC should also be relevant to experimental convective heat transfer. Experimental setups for obtaining discrete Green's functions/local influence coefficients are non-trivial, similarly restricted by the locality of Green's functions. In the SHTC framework, one may have a relatively simple and robust steady experimental setup. A solid wall may be heated/cooled in a sinusoidal form of different wave lengths and the corresponding heat fluxes can be measured once a sufficent thermal equilibrium state is reached. The influence coefficients in a spectral form (SHTC) for different wavelengths/modes can then be simply obtained respectively. The envisaged experimental setup should expectedly have much reduced experimental errors/uncertainties associated with the difficulties in achieving the locality required by Green's functions.

Further validations, demonstrations and applications are expected in future.

Author statement

I hereby declare that the work as documented in 'Spectral Heat Transfer Coefficient for Convection' is the author's own and has not been submitted to elsewhere for publication.

Declaration of Competing Interest

The authors declare that they have no known competing financial interests or personal relationships that could have appeared to influence the work reported in this paper.

Data availability

Data will be made available on request.

Acknowledgement

The author gratefully appreciates the vision and initiative in establishing the Statutory Chair of Computational Aerothermal Engineering

and the enlightening institutional environment of academic freedom and intellectual independence at Oxford, which have made the present work possible.

Appendix A. Equivalence of Half-range Fourier and Chebyshev spectral modelling

Start with the half-range Fourier series of N_F harmonics for a non-periodic function in a continuous angular domain ($0< \theta <\pi$). A function f can be expressed as:

$$f(\theta) = \sum_{n=0}^{N_F} a_n \cos n\theta = f_0 + \sum_{n=1}^{N_F} a_n \cos n\theta \tag{A.1}$$

$$a_n = \frac{2}{\pi}\int_0^{\pi} f(\theta) cos(n\theta) d\theta, (n = 1,\ 2,\ \ldots,\ N_F) \tag{A.2}$$

The corresponding discrete angular domain of N_D mesh cells is:

$$\theta_i = 2\pi i / N_D, (i = 1,\ 2,\ \ldots,\ N_D) \tag{A.3}$$

Then the discrete Fourier representation of f at point θ_i becomes:

$$f_i(\theta_i) = f_0 + \sum_{n=1}^{N_F} a_n \cos n\theta_i$$

The corresponding Fourier harmonic coefficients can be obtained by:

$$f_0 = \frac{1}{N_D}\sum_{i=1}^{N_D} f_i \tag{A.4a}$$

$$a_n = \frac{2}{N_D}\sum_{i=1}^{N_D} f_i cos(n\theta_i), (n = 1,\ 2,\ \ldots,\ N_F) \tag{A.4b}$$

Now we examine a Chebyshev spectral representation ('the polynomial of the first kind') for function f(x) in domain $(-1 < x < 1)$. For a polynomial of N_C degrees (Trefethen [34], Boyd [35]):

$$f(x) = \sum_{k=0}^{N_C} c_k T_k(\mathrm{x}) = f_0 + \sum_{k=1}^{N_C} c_k T_k(\mathrm{x}) \tag{A.5}$$

$$c_k = \frac{2}{\pi}\int_{-1}^{1} \frac{f(x) T_k(\mathrm{x})}{\sqrt{1-x^2}} dx \tag{A.6}$$

where c_k is the coefficient for kth degree and $T_k(\mathrm{x})$ is the corresponding basis function.

Take $x = \cos\varphi$, $(0 < \varphi < \pi)$, then it can be shown that Eq. (A.6) becomes, $c_k = \frac{2}{\pi}\int_0^{\pi} f(\cos\varphi) T_k(\cos\varphi) d\varphi$.

Given the definition of the polynomial of the first kind: $T_k(\cos\varphi) = \cos k\varphi$, we have: $c_k = \frac{2}{\pi}\int_0^{\pi} f(\cos\varphi)\cos(\mathrm{k}\varphi) d\varphi$.

Take the corresponding discrete angular domain of N_D mesh cells for φ as:

$$\varphi_j = 2\pi j / N_D, \quad (j = 1,\ 2,\ \cdots,\ N_D) \tag{A.7}$$

And f at discrete point φ_j is denoted as f_j, ($j = 1, 2, \ldots, N_D$), then the discrete form of the integral for the Chebyshev spectral coefficients becomes:

$$f_0 = \frac{1}{N_D}\sum_{j=1}^{N_D} f_j \tag{A.8a}$$

$$c_k = \frac{2}{N_D}\sum_{j=1}^{N_D} f_j cos(k\varphi_i), (k = 1,\ 2, \ldots,\ N_C) \tag{A.8b}$$

Comparing Eq. A.8 with Eq. A.4, we can see that if the number of harmonics (N_F) of the Fourier series is taken to be the same as the degrees (N_C) of the Chebyshev polynomial, coefficient c_k will then correspond exactly to a_n. Therefore, the two spectral representations are equivalent to each other.

Appendix B. SHTC formulations for three-dimensional applications

The SHTC formulations are introduced in the main text for a 2D domain with a 1D wall boundary for simplicity. Here we present the formulations for a 3D domain with a 2D wall boundary surface (Fig. 3). The same principal procedure as in the 2D setting also applies to a 3D setting. The key difference is that we will need to use a double Fourier series for a 3D case, rather than a single Fourier series in a 2D case.

Consider now a 3D fluid domain bounded by a solid wall with M_W mesh cells in the x direction and N_W mesh cells in the y direction respectively (Fig. 3). The wall temperatures are taken at the mesh cell centre points. Assume a spatial periodicity in both wall-parallel directions. The wall temperature disturbance distribution over the wall boundary can be represented by a double Fourier series retaining M_F harmonics in x and N_F harmonics in y respectively. Wall mesh points are indexed by i, j and the corresponding spatial locations are marked by angles α_i and β_j:

$$\alpha_i = 2\pi i/M_w, (i = 1,\ 2,\ \ldots,\ M_W) \tag{A.9}$$

$$\beta_j = 2\pi j/N_w\ (j = 1,\ 2,\ \ldots,\ N_W) \tag{A.10}$$

Wall temperature disturbance ΔT_{ij} for mesh cell i, j is expressed as

$$\Delta T_{ij} = \Delta T_0 + \sum_{m=0,\ n=0,\ (m+n\geq 1)}^{M_F,N_F} \Lambda_{mn}\left(A_{mn}\cos m\alpha_i \cos n\beta_j + B_{mn}\sin m\alpha_i \cos n\beta_j + C_{mn}\cos m\alpha_i \sin n\beta_j + D_{mn}\sin m\alpha_i \sin n\beta_j\right)$$

$$\Lambda_{mn} = \frac{1}{2}, (m = 0 \ and\ n > 0,\ or\ n = 0\ and\ m > 0)$$

$$\Lambda_{mn} = 1, (m > 0\ and\ n > 0) \tag{A.11}$$

ΔT_0 the zeroth harmonic is the spatial average over the entire boundary, thus a constant base for all wall mesh points equivalent to that for an isothermal case. The M_F x N_F harmonic spectrum is controlled by $(2M_F+1)$ $(2N_F+1)$ parameters, each corresponding to a Fourier mode. The wall temperature disturbance can also be expressed as a linear sum of $(2M_F+1)$ $(2N_F + 1)$ Fourier modes for the wall temperature at mesh point i,j:

$$\Delta T_{ij} = \Delta T_0 + \sum_{m=0,\ n=0\ (m+n\geq 1)}^{M_F,N_F} \left(\Delta T_{Amn} + \Delta T_{Bmn}\ +\ \Delta T_{Cmn} + \Delta T_{Dmn}\right)_{ij} \tag{A.12}$$

Correspondingly heat flux at mesh point i,j is decomposed to $(2M_F+1)$ $(2N_F + 1)$ modes respectively:

$$q_{ij} = q_{0ij} + \sum_{m=0,\ n=0,(m+n\geq 1)}^{M_F,N_F} \left(q_{Amn} + q_{Bmn}\ +\ q_{Cmn} + q_{Dmn}\right)_{ij} \tag{A.13}$$

The mode balance for the zeroth harmonic is similar to that in the 2D setting (Eq. (3.12)):

$$q_{0_{ij}} = H_{0_{ij}}\Delta T_0 \tag{A.14}$$

Now we see that the zeroth harmonic mode balance for a 3D case is also in exactly the same original form as Newton's law of cooling for an isothermal wall, as intended.

The Fourier mode balance for the mth harmonic in x and the nth harmonic in y now includes 4 components. Following the mode balance procedure similarly to a 2D case, now for mesh point i,j, we have:

$$q_{Amn_{ij}} = H_{Amn_{ij}}A_{mn} \tag{A.15a}$$

$$q_{Bmn_{ij}} = H_{Bmn_{ij}}B_{mn} \tag{A.15b}$$

$$q_{Cmn_{ij}} = H_{Cmn_{ij}}C_{mn} \tag{A.15c}$$

$$q_{Dmn_{ij}} = H_{Dmn_{ij}}D_{mn} \tag{A.15d}$$

We can then express the local heat flux at point i, j in form of a sum of $(2M_F+1)$ $(2N_F + 1)$ terms of corresponding Fourier spectral modes:

$$q_{ij} = H_{0_{ij}}\Delta T_0 + \sum_{m=0,\ n=0\ (m+n\geq 1)}^{M_F,N_F} \left(H_{Amn_{ij}}A_{mn} + H_{Bmn_{ij}}B_{mn} + H_{Cmn_{ij}}C_{mn} + H_{Dmn_{ij}}D_{mn}\right) \tag{A.16}$$

When we use the half-range Fourier series in both x and y directions, all terms involving sine functions will disappear. Effectively, we have only about a quarter of the original full range terms to be covered. The number of Fourier modes is then reduced from $(2M_F+1)$ $(2N_F + 1)$ to (M_F+1) $(N_F + 1)$. The problem size is reduced to about 25% of the full range one, so is the number of CFD solutions needed to fix the corresponding SHTC.

The working procedure will also be similar to that for a 2D situation.

Firstly, for the generation of the SHTC in a fluid-domain-only-setting, the zeroth harmonic (the overall average 'isothermal' mode) is exactly the same as that for the 2D. For the mth harmonic in x and the nth harmonic in y, we now have 4 modes for mesh point i,j:

a) CosineConsine mode: Specify $(\Delta T_{Amn})_{ij} = A_{mn}\cos(m\alpha_i)\cos(n\beta_j)$ and solve $(q_{Amn})_{ij}$; Postprocess $(H_{Amn})_{ij} = (q_{Amn})_{ij}/A_{mn}$
b) SineCosine mode: Specify $(\Delta T_{Bmn})_{ij} = B_{mn}\sin(m\alpha_i)\cos(n\beta_j)$ and solve $(q_{Bmn})_{ij}$; Postprocess $(H_{Bmn})_{ij} = (q_{Bmn})_{ij}/B_{mn}$
c) CosineSine mode: Specify $(\Delta T_{Cmn})_{ij} = C_{mn}\cos(m\alpha_i)\sin(n\beta_j)$ and solve $(q_{Cmn})_{ij}$; Postprocess $(H_{Cmn})_{ij} = (q_{Cmn})_{ij}/C_{mn}$
d) SineSine mode: Specify $(\Delta T_{Dmn})_{ij} = D_{mn}\sin(m\alpha_i)\sin(n\beta_j)$ and solve $(q_{Dmn})_{ij}$; Postprocess $(H_{Dmn})_{ij} = (q_{Dmn})_{ij}/D_{mn}$

Secondly, for a conduction solution with the SHTC in a solid-domain-only setting, the same procedure is followed as in the 2D setting. The main thing to note is the different discrete forms of the formulations in a 3D setting for those coefficients (magnitudes) of the Fourier modes for wall temperature disturbances:

$$\Delta T_0 = \frac{1}{M_w N_w}\sum_{i=1,j=1}^{M_w,N_w} \Delta T_{ij} \tag{A.17}$$

$$A_{mn} = \frac{4}{M_w N_w} \sum_{i=1,j=1}^{M_w,N_w} \Delta T_{ij} cos(m\alpha_i) cos\left(n\beta_j\right) \tag{A.18a}$$

$$B_{mn} = \frac{4}{M_w N_w} \sum_{i=1,j=1}^{M_w,N_w} \Delta T_{ij} sin(m\alpha_i) cos\left(n\beta_j\right) \tag{A.18b}$$

$$C_{mn} = \frac{4}{M_w N_w} \sum_{i=1,j=1}^{M_w,N_w} \Delta T_{ij} cos(m\alpha_i) sin\left(n\beta_j\right) \tag{A.18c}$$

$$D_{mn} = \frac{4}{M_w N_w} \sum_{i=1,j=1}^{M_w,N_w} \Delta T_{ij} sin(m\alpha_i) sin\left(n\beta_j\right) \tag{A.18d}$$

$(0 \le m \le M_F,\ 0 \le n \le N_F \ and \ m+n \ \ge 1)$

Again, when we adopt the half-range spectrum in both directions, only will A_{mn} (Eq. (A.18a)) need to be retained, the other three in Eq. A.18 are all zero, leading to a very significant reduction in computing effort required.

References

[1] R.J. Moffat, What's new in convective heat transfer? Int. J. Heat Fluid Flow 19 (1998) 90–101.
[2] R. Maffulli, L. He, Wall temperature effects on heat transfer coefficient for high pressure turbines, AIAA J. Propuls. Power 30 (4) (2014) 1080–1090, 2014.
[3] Q. Zhang, L. He, Impact of wall temperature on turbine blade tip aero-thermal performance, J. Eng. Gas Turbines Power 136 (5) (2014), 052602.
[4] R. Maffulli, L. He, Impact of wall temperature on heat transfer coefficient and aerodynamics for three-dimensional turbine blade passage, J. Therm. Sci. Eng. Appl. 9 (4) (2017), 041002.
[5] F. Vocale, F. Bozzoli, S. Rainieri, G. Pagliarini, Influence of thermal boundary conditions on local convective heat transfer in coiled tubes, Int. J. Therm. Sci. 145 (2019), 106039.
[6] F. Bozzoli, L. Cattani, S. Rainieri, G. Pagliarini, Estimation of local heat transfer coefficient in coiled tubes under inverse heat conduction problem approach, Exp. Therm. Fluid Sci. 59 (2014) 246–251.
[7] M. Ciofalo, M.F. La Cerva, M. Di Liberto, A. Tamburin, Influence of the boundary conditions on heat and mass transfer in spacer-filled channels, J. Phys. Conf. Ser. 923 (2017), 012054.
[8] J.A. Ruffner, Reinterpretation of the genesis of Newton's "Law of Cooling, Arch. Hist. Exact Sci. 2 (2) (1963) 138–152.
[9] G.W. Molnar, Newton's thermometer: a model for testing Newton's law of cooling, Physiologist 12 (1) (1969) 9–19.
[10] U. Grigull, Newton's temperature scale and the law of cooling, Wärme Stoffübertrang. 18 (1984) 195–199, 1984.
[11] C.T. O'Sullivan, Newton law of cooling–a critical assessment, Am. J. Phys. 58 (10) (1990) 956–960.
[12] U. Besson, The history of the Cooling Law: when the search for simplicity can be an obstacle, Sci. Educ. 21 (2012) 1085–1110, 2012.
[13] S. Maruyama, S. Moriya, Newton's Law of cooling: follow up and exploration, Int. J. Heat Mass Transf. 164 (2021), 120544.
[14] J. Hacker, J. Eaton, Measurements of heat transfer in a separated and reattaching flow with spatially varying thermal boundary conditions, Int. J. Heat Fluid Flow 18 (1) (1997) 131–141, 1997.
[15] A.M. Anderson, R.J. Moffat, The adiabatic heat transfer coefficient and the superposition kernel function: part 1–data for arrays of flatpacks for different flow conditions, ASME J. Electron. Packag. 114 (1) (1992) 14–21.
[16] K.A. Batchelder, J.K. Eaton, Practical experience with the discrete Green's function approach to convective heat transfer, J. Heat Transf. 123 (1) (2000) 70–76.
[17] C.W. Booten, J.K. Eaton, Discrete Green's function measurements in internal flows, J. Heat Transf. 127 (7) (2005), 692–69.
[18] D. Mukerji, J.K. Eaton, Discrete Green's function measurements in a single passage turbine model, J. Heat Transf. 127 (4) (2005) 366–377.
[19] V. Andreoli, D.G. Cuadrado, G. Paniagua, Prediction of the turbine tip convective heat flux using discrete Green's functions, J. Heat Transf. 140 (7) (2018), 071703.
[20] J. Saavedra, V. Athmanathan, G. Paniagua, T. Meyer, D. Straub, J. Black, Scalable heat transfer characterization on film cooled geometries based on discrete Green's functions, J. Turbomach. 143 (2) (2021).
[21] J.K. Eaton, The discrete Green's function for convective heat transfer–part 1: definition and physical understanding, J. Heat Transf. 142 (1) (2020), 102101.
[22] D.W. Hoffman, J.K. Eaton, Conjugate heat transfer analysis using the discrete Green's function, J. Heat Transf. 143 (2) (2021), 031401.
[23] L. He, Conjugate Heat Transfer: Some Fundamentals and Recent Progress, Chapter Two, Advances in Heat Transfer, 55, Elsevier, 2023, pp. 41–87.
[24] L. He, W. Ning, Efficient approach for analysis of unsteady viscous flows in turbomachines, AIAA J. 36 (11) (1998) 2005–2012.
[25] K.C. Hall, J.P. Thomas, W.S. Clark, Computation of unsteady nonlinear flows in cascades using a harmonic balance technique, AIAA J. 40 (5) (2002).
[26] L. He, Fourier methods for turbomachinery applications, Prog. Aerosp. Sci. 46 (8) (2010) 329–341.
[27] L. He, Closely coupled fluid-solid interface method with moving-average for LES based conjugate heat transfer solution, Int. J. Heat Fluid Flow 79 (2019), 108440.
[28] L. He, Two-scale conjugate heat transfer solution for micro-structured surface, Int. J. Numer. Methods Fluids 95 (8) (2023) 1260–1285.
[29] L. He, Fourier spectral method for multi-scale aerothermal analysis, Int. J. Comut. Fluid Dyn. 27 (2) (2013) 118–129.
[30] C. Chen, L. He, Two-scale solution for tripped turbulent boundary layer, J. Fluid Mech. 955 (2023) A5.
[31] T.L. Perelman, On conjugated problems of heat transfer, Int. J. Heat Mass Transf. 3 (4) (1961) 293–303.
[32] L. He, M.L.G. Oldfield, Unsteady conjugate heat transfer modelling, J. Turbomach. 133 (3) (2011).
[33] D.L. Schultz, T.V. Jones, Heat transfer measurement in short duration facilities, AGARD AG-165, 1973.
[34] L.N. Trefethen, Spectral Methods in MATLAB, SIAM, Philadelphia, 2000.
[35] J.P. Boyd, Chebyshev and Fourier Spectral Methods, Dover Publications, New York, 2001.